Retardation effects on intra- and intersubband plasmons in quantum wells and their manifestations in grating-coupler-assisted optical transmission

L. Wendler
Anna-Siemsen-Straße 66, D-07745 Jena, Germany

T. Kraft
Schlehenstraße 10, D-16321 Bernau, Germany

(Received 13 May 1998)

The dispersion relations of intra- and intersubband plasmon polaritons in quantum wells are investigated in the small wave-vector region. It is shown that the intrasubband plasmon polariton is a normal mode of the layered semiconductor microstructure for all wave vectors. The intersubband plasmon polariton, however, appears in two branches. The higher-frequency branch is a radiative virtual mode and the lower-frequency branch is a normal mode. It is shown that the normal modes appear as maxima and the virtual mode as a minimum in the relative transmission spectra of samples with a grating coupler above the electron system. Thus, the well-known deformation of the transmission line shape of the intersubband plasmon mode from a maximum for smaller grating periods to a minimum for larger grating periods is explained by the excitation of the radiative virtual intersubband plasmon polariton above the onset of the Rayleigh anomaly.
[S0163-1829(99)14031-1]

Electron-gas systems have well-defined collective modes of charge-density oscillations, the plasmons. Their dispersion relations characteristically depend on the dimensionality of the system. These collective excitations give rise to effects observable in a variety of physical situations. Thus, the properties of interacting electron systems and their collective excitations are of fundamental interest. The ability to grow modulation-doped semiconductor structures made possible the study of quasi-two-dimensional electron gas (Q2DEG) systems. Q2D plasmons have been investigated theoretically (see, e.g., Refs. 1–8) and experimentally (see, e.g., Refs. 9–16). Caused by the size quantization, the collective excitation spectrum becomes split in intrasubband plasmons, connected with collective (coherent) electron motion within one subband, and intersubband plasmons, connected with collective electron motion between two different subbands. Typically, these collective electron motions are not independent, and thus, due to the intersubband coupling (ISC), the mode spectrum is of hybrid type.

As shown in Refs. 3 and 7, retardation effects influence the modes only in a very narrow range around the dispersion relation of light $\omega = cq_\parallel/\sqrt{\varepsilon_b}$ [$\mathbf{q}_\parallel = (q_x, q_y)$, 2D wave vector, $q_\parallel = |\mathbf{q}_\parallel|$; ε_b, background dielectric constant; c, vacuum speed of light]. However, this is the region of the most optical experiments. Far-infrared (FIR) transmission spectroscopy is a very profitable method to study the Q2D plasmons.[9,10,12,14] However, if FIR radiation is applied to a semiconductor microstructure, it cannot couple directly to the normal modes of this system. This is true because the Q2D plasmons exist for $q_\parallel > \sqrt{\varepsilon_b}\omega/c$, but the accessible in-plane wave vector in a FIR experiment is $q_\parallel = (\omega/c)\sin\Theta_0$, where Θ_0 is the ray angle of the incident wave. In this case one can only excite radiative modes, which are virtual modes. Thus, for a Q2DEG in samples with flat surfaces, only the so-called collective intersubband resonances, existing for $q_\parallel < \sqrt{\varepsilon_b}\omega/c$, are observable. The investigation of the Q2D plasmon dispersion relation is only possible with the help of a grating coupler, generating in-plane wave vector components $q_\parallel = (\omega/c)\sin\Theta_0 + (2\pi/d)n$; $n = 0, \pm 1, \pm 2, \ldots$ perpendicular to the stripes of the grating with periodicity d[16–18] and, henceforth, couple the incident light with the plasmons that become by this way radiative modes. This shows quite generally that the FIR optical properties are related only to the radiative modes of the system and not to the nonradiative normal modes. Thus, it is important to analyze very carefully the collective excitations in the near vicinity (left and right) of the light line.

The current-response theory, describing the linear response of the system, gives the relation between the externally applied vector potential $\mathbf{A}^{\mathrm{ext}}$ and the induced vector potential $\mathbf{A}^{\mathrm{ind}}$,[7]

$$A_\alpha(\mathbf{q}_\parallel; z|\omega) = A_\alpha^{\mathrm{ext}}(\mathbf{q}_\parallel; z|\omega) + \mu_0 \sum_{\beta\gamma} \int dz' \int dz'' D_{\alpha\beta}(\mathbf{q}_\parallel; z, z'|\omega) \times P_{\beta\gamma}(\mathbf{q}_\parallel; z', z''|\omega) A_\gamma(\mathbf{q}_\parallel; z''|\omega), \quad (1)$$

where $\mathbf{A}(\mathbf{q}_\parallel; z|\omega) = \mathbf{A}^{\mathrm{ext}}(\mathbf{q}_\parallel; z|\omega) + \mathbf{A}^{\mathrm{ind}}(\mathbf{q}_\parallel; z|\omega)$ is the total vector potential, $P_{\alpha\beta}(\mathbf{q}_\parallel; z, z|\omega)$ are the components of the irreducible (proper) polarization tensor, $\alpha, \beta = x, y, z$, μ_0 is the permeability in vacuum, and $D_{\alpha\beta}(\mathbf{q}_\parallel; z, z'|\omega)$ is the Green's tensor of the inhomogeneous wave equation (for details see Ref. 7). This equation gives the dispersion relation of the collective excitations in random-phase approximation (RPA) including retardation, i.e., of the Q2D intra- and intersubband plasmon polaritons (coupled plasmon-photon modes), in the form

$$\det\left[\delta_{\alpha\gamma}\delta_{KK_1}\delta_{K'K_2}-\mu_0\sum_{\beta}D_{\alpha\beta}^{K_1K_2K'K}(\mathbf{q}_\parallel,\omega)P_{\beta\gamma}^{KK'}(\mathbf{q}_\parallel,\omega)\right]=0. \tag{2}$$

Herein, $P_{\alpha\beta}^{KK'}(\mathbf{q}_\parallel,\omega)$ is the matrix polarization tensor of the Q2DEG in RPA (Ref. 7) and $D_{\alpha\beta}^{K_1K_2K'K}(\mathbf{q}_\parallel,\omega)$ are the matrix elements of the Green's tensor of the inhomogeneous wave equation assuming envelope wave functions $\varphi_K(z)$ and subband energies $\mathcal{E}_K(\mathbf{k}_\parallel)=\mathcal{E}_K+\hbar^2\mathbf{k}_\parallel^2/(2m_e)$ of the quantum well (QW) containing the Q2DEG ($K=0,1,2,\ldots$; m_e, effective conduction-band-edge mass).

In the following, we restrict on *p*-polarized Q2D plasmon polaritons, assuming without loss on generality $\mathbf{q}_\parallel=(q_x,0)$, and consider the two lowest-frequency plasmon polaritons of the Q2DEG in the electric quantum limit (only the lowest subband is occupied) neglecting the intersubband coupling by using the diagonal approximation, i.e., only the (0-0) intrasubband plasmon polariton and the (1-0) intersubband plasmon polariton are considered. All these approximations are well satisfied for usual QW's, used in experiments (see, e.g., discussions in Refs. 6 and 7). In this case, the dispersion relation of the (0-0) intrasubband plasmon polariton follows from Eq. (2) in the form

$$1-\mu_0 D_{xx}^{00}(\mathbf{q}_\parallel,\omega)\chi_{xx}^0(\mathbf{q}_\parallel,\omega)=0. \tag{3}$$

This dispersion relation represents the independent collective electron motion in subband $\mathcal{E}_0(\mathbf{k}_\parallel)$. The dispersion relation of the (1-0) intersubband plasmon polariton is given by

$$1-\mu_0 D_{zz}^{11}(\mathbf{q}_\parallel,\omega)\chi_{zz}^1(\mathbf{q}_\parallel,\omega)=0, \tag{4}$$

which represents the independent collective electron motion between the subbands $\mathcal{E}_0(\mathbf{k}_\parallel)$ and $\mathcal{E}_1(\mathbf{k}_\parallel)$. Herein, we have defined $D_{\alpha\beta}^{KK'}(\mathbf{q}_\parallel,\omega)\equiv D_{\alpha\beta}^{K0K'0}(\mathbf{q}_\parallel,\omega)$, $\chi_{xx}^0(\mathbf{q}_\parallel,\omega)\equiv P_{xx}^{00}(\mathbf{q}_\parallel,\omega)$, and $\chi_{zz}^1(\mathbf{q}_\parallel,\omega)\equiv P_{zz}^{10}(\mathbf{q}_\parallel,\omega)+P_{zz}^{01}(\mathbf{q}_\parallel,\omega)$. It is important to note that $D_{\alpha\beta}^{KK'}(\mathbf{q}_\parallel,\omega)$ contains direct and image parts for layered systems in which the materials have different polarizabilities. Further, in deriving Eq. (4) we kept only the term $D_{zz}^{11}\chi_{zz}^1$, because all the other terms are in higher order of $\mathbf{q}_\parallel$. This is possible because we are interested in the range of small wave vectors $\mathbf{q}_\parallel$, where the long-wavelength approximation (LWA) is well fulfilled: $q_\parallel k_F^{(0)}\ll 1$ and $q_\parallel a_{2\mathrm{DEG}}\ll 1$ [$k_F^{(0)}=(2\pi n_{2\mathrm{DEG}})^{1/2}$, Fermi wave vector of subband $\mathcal{E}_0(\mathbf{k}_\parallel)$; $n_{2\mathrm{DEG}}$, electron number per unit area; $a_{2\mathrm{DEG}}$, effective thickness of the Q2DEG]. Using the LWA expressions[7]

$$\chi_{xx}^0(\mathbf{q}_\parallel,\omega)=-\frac{n_{2\mathrm{DEG}}e^2}{m_e}, \tag{5}$$

$$\chi_{zz}^1(\mathbf{q}_\parallel,\omega)=-\frac{n_{2\mathrm{DEG}}e^2}{m_e}\left[\frac{\hbar}{2m_e\Omega_{10}}\frac{\omega^2}{\omega^2-\Omega_{10}^2}\right], \tag{6}$$

$$D_{xx}^{00}(\mathbf{q}_\parallel,\omega)=-\frac{c^2\alpha_\nu}{2\varepsilon_{b\nu}\omega^2}\{1+\mathcal{S}(\mathbf{q}_\parallel,\omega)+\alpha_\nu[\alpha_{00}+\mathcal{S}(\mathbf{q}_\parallel,\omega)\overline{\alpha}_{00}]\}, \tag{7}$$

and

$$D_{zz}^{11}(\mathbf{q}_\parallel,\omega)=-\frac{c^2}{2\varepsilon_{b\nu}\omega^2}\left(\frac{2m_e\Omega_{10}}{\hbar}\right)^2\times\left\{\alpha_{11}-\frac{q_\parallel^2}{\alpha_\nu}[\beta_{11}+\mathcal{S}(\mathbf{q}_\parallel,\omega)\overline{\beta}_{11}]\right\} \tag{8}$$

in Eqs. (3) and (4), it follows for the *p*-polarized (0-0) intrasubband plasmon polariton

$$\omega_{pp}^{00}=\left\{\frac{n_{2\mathrm{DEG}}e^2}{2m_e\varepsilon_0\varepsilon_{b\nu}}\alpha_\nu(1+\mathcal{S}(\mathbf{q}_\parallel,\omega_{pp}^{00})+\alpha_\nu[\alpha_{00}+\mathcal{S}(\mathbf{q}_\parallel,\omega_{pp}^{00})\overline{\alpha}_{00}])\right\}^{1/2} \tag{9}$$

and for the *p*-polarized (1-0) intersubband plasmon polariton

$$\omega_{pp}^{10}=\left\{\Omega_{10}^2+\frac{n_{2\mathrm{DEG}}e^2\Omega_{10}}{\hbar\varepsilon_0\varepsilon_{b\nu}}\times\left(\alpha_{11}-\frac{q_\parallel^2}{\alpha_\nu}[\beta_{11}+\mathcal{S}(\mathbf{q}_\parallel,\omega_{pp}^{10})\overline{\beta}_{11}]\right)\right\}^{1/2}. \tag{10}$$

Equation (9) determines the frequency $\omega=\omega_{pp}^{00}(\mathbf{q}_\parallel)$ of the (0-0) intrasubband plasmon-polariton mode and Eq. (10) that of the (1-0) intersubband plasmon-polariton mode $\omega=\omega_{pp}^{10}(\mathbf{q}_\parallel)$. In the above equations, ε_0 is the permittivity in vacuum, $\varepsilon_{b\nu}$ is the background dielectric constant ($\nu=1,2,3,\ldots$ denotes the different layers) of that layer in which the Q2DEG is quantum confined, and $\alpha_\nu=(q_\parallel^2-\varepsilon_{b\nu}\omega^2/c^2)^{1/2}$. Further, we have defined $\alpha_{KK}=-\langle\varphi_K\varphi_0|z-z'\|\varphi_K\varphi_0\rangle$, $\overline{\alpha}_{KK}=-\langle\varphi_K\varphi_0|(z+z')|\varphi_K\varphi_0\rangle$, $\beta_{KK}=(-1/2)\langle\varphi_K\varphi_0\|z-z'|^2|\varphi_K\varphi_0\rangle$, and $\overline{\beta}_{KK}=(-1/2)\langle\varphi_K\varphi_0|(z+z')^2|\varphi_K\varphi_0\rangle$, which depend on the shape of the confining potential forming the QW for the Q2DEG. $\Omega_{10}=(\mathcal{E}_1-\mathcal{E}_0)/\hbar$ is the subband separation frequency, and $\mathcal{S}(\mathbf{q}_\parallel,\omega)$ is a geometry factor, which is responsible for image effects and depends on the concrete form of the multilayer system.[6] For instance, one has $\mathcal{S}(\mathbf{q}_\parallel,\omega)=0$ in the absence of image effects. For the model system in which region $\nu=0$ ($0<z$) is filled by vacuum, layer $\nu=1$ of thickness d_1 ($-d_1<z<0$) is filled by a material characterized by ε_{b1} (e.g., by a metal simulating a gate on top of the sample), layer $\nu=2$ has a finite thickness d_2 ($-(d_1+d_2)<z<-d_1$) and is filled with a material (e.g., the wider-gap semiconductor) characterized by ε_{b2}, and region $\nu=3$ ($z<-(d_1+d_2)$) is filled with a material (e.g., the smaller-gap semiconductor) characterized by the background dielectric constant ε_{b3} and contains the QW, one has

$$\mathcal{S}(\mathbf{q}_\parallel,\omega)=\frac{r_{23}+\tilde{r}_{012}\exp(-2\alpha_2 d_2)}{1+\tilde{r}_{012}\,r_{23}\exp(-2\alpha_2 d_2)}\exp[2\alpha_3(d_1+d_2)],$$

where

$$\tilde{r}_{012}=\frac{r_{12}+r_{01}\exp(-2\alpha_1 d_1)}{1+r_{01}\,r_{12}\exp(-2\alpha_1 d_1)}$$

and

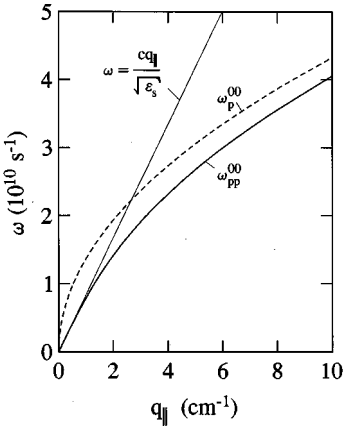

FIG. 1. Dispersion relations of the (0-0) intrasubband plasmon polariton ω_{pp}^{00} (heavy solid line) and of the (0-0) intrasubband plasmon ω_p^{00} (dashed line) in dependence on the 2D wave vector. The LWA dispersion curves are calculated from Eqs. (9) and (11).

$$\frac{r_{ij}=[\varepsilon_{bj}\alpha_i-\varepsilon_{bi}\alpha_j]}{[\varepsilon_{bj}\alpha_i+\varepsilon_{bi}\alpha_j]}.$$

In the absence of the metal film, we have

$$\mathcal{S}(\mathbf{q}_\parallel,\omega)=\tilde{r}_{023}\exp(2\alpha_3 d_2)$$
$$=\frac{r_{23}+r_{02}\exp(-2\alpha_2 d_2)}{1+r_{02}\,r_{23}\exp(-2\alpha_2 d_2)}\exp(2\alpha_3 d_2)$$

and for a half-space geometry with the semi-infinite region 2 ($0<z$) and the semi-infinite region 3 ($z<0$), it follows $\mathcal{S}(\mathbf{q}_\parallel,\omega)=r_{23}$.

If one neglects retardation effects, $c\to\infty$, one obtains from Eqs. (9) and (10) the explicit LWA dispersion relations of the (0-0) intrasubband plasmon

$$\omega_p^{00}=\left\{\frac{n_{2\mathrm{DEG}}e^2}{2m_e\varepsilon_0\varepsilon_{bv}}q_\parallel(1+\mathcal{S}(\mathbf{q}_\parallel)+q_\parallel[\alpha_{00}+\mathcal{S}(\mathbf{q}_\parallel)\overline{\alpha}_{00}])\right\}^{1/2} \tag{11}$$

and that of the (1-0) intersubband plasmon

$$\omega_p^{10}=\left\{\Omega_{10}^2+\frac{n_{2\mathrm{DEG}}e^2\Omega_{10}}{\hbar\varepsilon_0\varepsilon_{bv}}(\alpha_{11}-q_\parallel[\beta_{11}+\mathcal{S}(\mathbf{q}_\parallel)\overline{\beta}_{11}])\right\}^{1/2}, \tag{12}$$

which are the original LWA results of the corresponding density-response scheme (see, e.g., Refs. 6 and 7). Please note that the associated $\mathcal{S}(\mathbf{q}_\parallel)$ follows from $\mathcal{S}(\mathbf{q}_\parallel,\omega)$ for $\alpha_i\to q_\parallel$. While the intrasubband plasmon starts for $q_\parallel=0$ at $\omega=0$ because of the vanishing restoring force, the intersubband plasmon starts for $q_\parallel=0$ above the subband separation frequency Ω_{10}. This frequency shift $\Delta_p^{10}=\omega_p^{10}(\mathbf{q}_\parallel=0)-\Omega_{10}$ is the depolarization shift.

The dispersion curves of the (0-0) intrasubband and (1-0) intersubband plasmons and that of the associated plasmon polaritons are plotted in Figs. 1 and 2, respectively, neglecting image effects. For numerical calculation we have chosen a GaAs-$Ga_{1-x}Al_xAs$ single heterostructure (SHS) (GaAs, $\varepsilon_{bv}\equiv\varepsilon_s=12.87$; ε_s, static dielectric constant and $m_e=0.0662m_0$; m_0, bare electron mass) with a triangular-well confining potential. The Q2DEG in the SHS we have

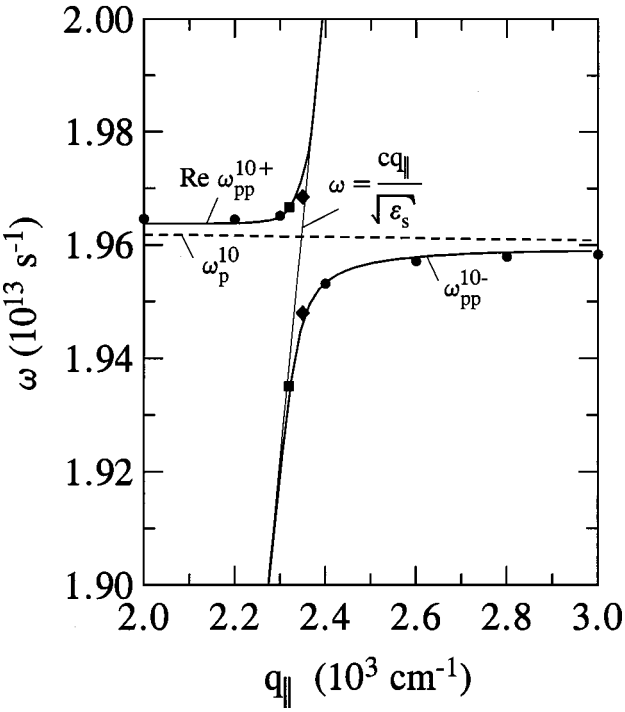

FIG. 2. Dispersion relations of the (1-0) intrasubband plasmon polariton $\omega_{pp}^{10\pm}$ (heavy solid line) and of the (1-0) intrasubband plasmon ω_p^{10} (dashed line) in dependence on the 2D wave vector. The LWA dispersion curves are calculated from Eqs. (10) and (12). As mentioned in the text for the upper branch, Reω_{pp}^{10+} is plotted. The symbol (●) denotes the positions of the maxima and minima in the relative transmission spectra of Fig. 4, and the symbols (■) and (♦) denote those of Fig. 5 for $\Theta_0=1.749°$ and $\Theta_0=4.377°$, respectively.

characterized by: $\varphi_0(z)=2\kappa_0^{3/2}\overline{z}e^{-\kappa_0\overline{z}}$, $\varphi_1(z)=2\kappa_2^{3/2}\overline{z}(1-\kappa_3\overline{z})e^{-\kappa_1\overline{z}}$, where $\overline{z}=-z-(d_1+d_2)$, $\kappa_0=1/(z_0-d)$, $\kappa_1=-[(z_0-z_1)\kappa_0+3]/(z_0-z_1)$, $\kappa_2=[12\kappa_1^5/(\kappa_0^2-\kappa_0\kappa_1+\kappa_1^2)]^{1/3}$, and $\kappa_3=(\kappa_0+\kappa_1)/3$, with $d=[\hbar^2/(2m_eeF)]^{1/3}$, $z_K=\mathcal{E}_K/(eF)$, and $\mathcal{E}_K=eFdx_K$, where x_K are the zeros of the Airy function, $F=e(n_{2\mathrm{DEPL}}+fn_{2\mathrm{DEG}})/(\varepsilon_0\varepsilon_s)$, and we have used $f=0.3$, $n_{2\mathrm{DEG}}=1\times10^{11}$ cm^{-2} for the electron concentration, and for the concentration of the depletion charges $n_{2\mathrm{DEPL}}=5\times10^9$ cm^{-2} (for details see Ref. 6) in the numerical analysis. With these envelope wave functions, one obtains $\alpha_{00}=-15/(16\kappa_0)$, $\overline{\alpha}_{00}=-3/\kappa_0$, $\alpha_{11}=5(\kappa_0\kappa_2)^3/(\kappa_0+\kappa_1)^7$, and $\beta_{11}=16(\kappa_0\kappa_2)^3/(\kappa_0+\kappa_1)^8=-\overline{\beta}_{11}$.

If retardation is included, it is found that both modes are affected. It becomes obvious from Figs. 1 and 2 that the intersubband mode is more drastically modified than the intrasubband mode. It is seen that in comparison to the nonretarded solution ω_p^{00} the dispersion curve of the intrasubband plasmon polariton ω_{pp}^{00} is slightly pushed down, so that it always lies to the right of the light line $\omega=cq_\parallel/\sqrt{\varepsilon_s}$ (in the absence of image effects only this once light line is present). This is true because Eq. (9) has only a real solution ω_{pp}^{00}, and henceforth, ω_{pp}^{00} is a nonradiative normal mode of the system with electromagnetic fields decaying exponentially from the surfaces of the sample into the surrounding medium. For larger wave vectors, ω_{pp}^{00} approaches ω_p^{00}.

The dispersion curve of the intersubband plasmon polar-

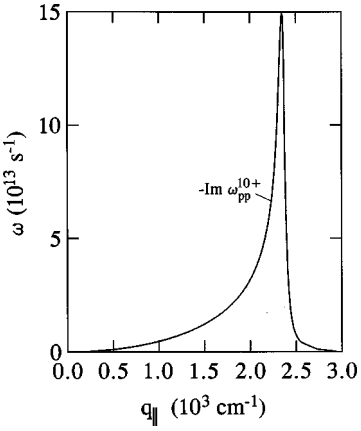

FIG. 3. $-\mathrm{Im}\,\omega_{pp}^{10+}$ as a function of the 2D wave vector calculated from Eq. (10).

iton, by contrast, is split into two branches ω_{pp}^{10+} and ω_{pp}^{10-}. These two branches ω_{pp}^{10+} and ω_{pp}^{10-} arise due to the anticrossing effect of the mode ω_p^{10} with the photon dispersion relation $\omega = cq_\parallel/\sqrt{\varepsilon_s}$ to form the coupled (hybrid) (1-0) intersubband plasmon-photon mode. The lower branch lies just below the light line and goes to the asymptote ω_p^{10} for larger wave vectors $q_\parallel$. It corresponds to the real solution of Eq. (10), and therefore, ω_{pp}^{10-} is a nonradiative normal mode of the system with electromagnetic fields decaying exponentially from the surfaces of the sample into the surrounding medium. Usually this branch is called the intersubband plasmon (polariton). The implicit equation has a second solution ω_{pp}^{10+}, which is complex. Here we assume $q_\parallel$ to be real and ω_{pp}^{10+} to be complex, i.e., we assume a pure temporal damping. It is noteworthy that this choice acts as a boundary condition for the radiative exit channel. In Ref. 19 it was shown quite generally that with this boundary condition for the radiative exit channel one selects different types of virtual modes describing different (experimental) situations. In the region $q_\parallel < \sqrt{\varepsilon_s}\omega/c$, real photons can couple with the intersubband mode, and thus, the branch ω_{pp}^{10+} is a radiative virtual mode, which decays by radiating energy into the surrounding medium, i.e., it has a finite lifetime. Henceforth, in a FIR transmission experiment performed in the absence of a grating coupler only this virtual mode, which is usually called collective intersubband resonance (dimensional resonance), is excited and the transmission spectrum exhibits a minimum at the position $\omega = \mathrm{Re}\,\omega_{pp}^{10+}$. The resonance splitting is $\mathrm{Re}\,\omega_{pp}^{10+} - \mathrm{Re}\,\omega_{pp}^{10-} \approx 1.76\times 10^{11}\ \mathrm{s}^{-1}$ for the chosen parameters. It is noteworthy that it was predicted long ago by Ferrell[20] that (classical) plasma oscillations in a metal film that involve motion normal to the slab can radiate. It is seen from Fig. 3 that $|\mathrm{Im}\,\omega_{pp}^{10+}|$ is zero for $q_\parallel$, increases with increasing wave vector, and shows a pronounced maximum at a finite wave vector. For larger wave vectors, $|\mathrm{Im}\,\omega_{pp}^{10+}|$ rapidly tends to zero. Comparing Figs. 2 and 3, it becomes obvious that the condition to denote ω_{pp}^{10+} as a mode, i.e., the condition of a weak damping, $\mathrm{Re}\,\omega_{pp}^{10+} \gg |\mathrm{Im}\,\omega_{pp}^{10+}|$, is fulfilled for $q_\parallel < 1.5\times 10^3\ \mathrm{cm}^{-1}$ and for $q_\parallel > 2.5\times 10^3\ \mathrm{cm}^{-1}$. Thus, for $q_\parallel = 0$ no radiative damping is present, and for small wave vectors, the radiative damping of ω_{pp}^{10+} is not very strong. This is the deeper physical reason why in FIR transmission experiments, where only this small wave-vector region is accessible, the intersubband resonance shows a relatively sharp peak in the spectrum.

It is interesting to note that in the earlier work of Kliewer and Fuchs[21,22] on phonon-polaritons of macroscopically thick slabs virtual modes with similar properties were found. Thus, summarizing the properties of ω_{pp}^{00} and $\omega_{pp}^{10\pm}$, it seems that the intra- and intersubband plasmon polaritons of a semiconductor heterostructure behave like the surface plasmon polaritons of a macroscopically thick metal or doped semiconductor layer (see, e.g., Refs. 23–25). In this case two nonradiative branches exist right to the light line, approaching for large wave vectors the asymptote $\omega_p/\sqrt{2}$ [$\omega_p = (n_{3\mathrm{DEG}}e^2/(\varepsilon_0\varepsilon_b m_e))^{1/2}$, 3D plasma frequency], and start at $q_\parallel = 0$ at $\omega = 0$. The so-called upper mode (also called high-frequency or ''normal'' mode) is antisymmetric, and the lower mode (low-frequency or ''tangential'' mode) is symmetric, analogous as the intra- and intersubband plasmon modes, respectively. The (macroscopic) surface modes are accompanied by surface polarization charges only. For the upper mode an excess of charge density at a point on one surface is accompanied by a deficiency at a point directly across the slab on the other surface, while the lower mode is accompanied by a symmetric disposition of charge excess or deficiency at opposing points on the two surfaces. Whereas the nonradiative normal modes of a macroscopically thick slab are Fano-type modes, the radiative branch, existing to the left of the light line, is a Brewster-type mode. Its real part of the frequency starts for $q_\parallel = 0$ at $\omega = \omega_p$ and approaches $\omega = cq_\parallel/\sqrt{\varepsilon_b}$ for larger wave vectors. Further, like for the dispersion relation of the intersubband plasmon mode, if retardation is neglected, the upper mode has one branch that starts for $q_\parallel = 0$ at $\omega = \omega_p$ and approaches $\omega_p/\sqrt{2}$ for large $q_\parallel$. Thus, we conclude that for small wave vectors the Q2D plasmon modes ω_{pp}^{00} and $\omega_{pp}^{10\pm}$ behave like the lower and the upper surface mode of a macroscopically thick slab.

Up to now we have investigated the collective excitations of the freely oscillating Q2DEG. The question, which we now elaborate, is how these collective excitations manifest in optical spectra. Of special interest is the coupling of incident FIR light with the (1-0) intersubband plasmon mode, on which we concentrate in the following. Because the investigation of normal modes is not directly accessible in FIR spectroscopy, one uses a grating coupler of period d, which generates in-plane wave-vector components $q_\parallel = (\omega/c)\sin\Theta_0 + (2\pi/d)n$; $n = 0, \pm 1, \pm 2, \ldots$ perpendicular to the stripes of the grating and converts the in-plane components of the incident electromagnetic field in the perpendicular component. By this way, the grating produces the (infinite) set of light lines $\omega = (c/\sqrt{\varepsilon_s})\,|q_\parallel + (2\pi/d)n|$ forming light cones centered at $q_\parallel = -(2\pi/d)n$. Consequently, the portions of a dispersion curve of the sample without the grating lying inside these light cones, i.e., for $\omega > (c/\sqrt{\varepsilon_s})\,|q_\parallel + (2\pi/d)n|$, become radiative. The periodicity of the grating may influence the dispersion curves of the freely propagating modes itself: due to the Bragg scattering of the modes and the resulting mode coupling minigaps may occur at $q_\parallel = (\pi/d)n$ (see, e.g., Ref. 26 for the theory of classical surface polaritons on periodic surface profiles; Ref. 27 for a recent experiment on surface plasmon polaritons on

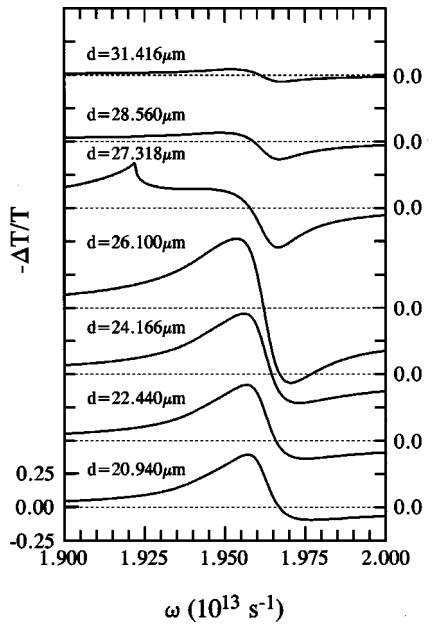

FIG. 4. Calculated relative transmission coefficient $-\Delta T/T$ of the multilayer system in the near vicinity of the (1-0) intersubband plasmon mode (''intersubband resonance'') for $\Theta_0=0°$ and different periods d of the grating.

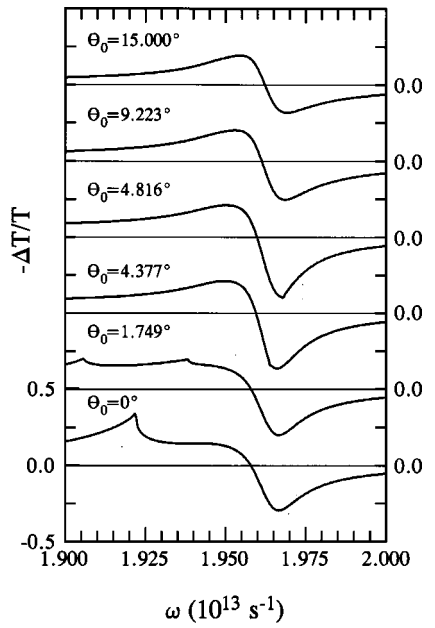

FIG. 5. Calculated relative transmission coefficient $-\Delta T/T$ of the multilayer system in the near vicinity of the (1-0) intersubband plasmon mode (''intersubband resonance'') for $d=27.318$ μm and different ray angles Θ_0.

a Ag surface textured with a hexagonal array of dots and Ref. 28 for experiments on 2D plasmons in the presence of a grating spatially modulating the 2DEG). The following results are obtained with our theory of the grating-coupler-induced optical response of multilayer systems of anisotropic media (for details, see Refs. 17 and 18). This theory describes both effects, possible resonance splitting of the modes due to retardation and Bragg scattering. Which of them occurs in the spectra strongly depends on the parameters under consideration. For the sample used here, we expect the width of possible minigaps much below the theoretical resolution of the calculated spectra. Therefore, we use the grating coupler only as measuring device to open additional radiative exit channels, i.e., we assume for the further discussion a nearly vanishing influence of the grating on the ''flat surface dispersion curves.''

The numerical calculations are done for the following model system: region $\nu=0$ $(0<z)$ is filled by vacuum. Layer $\nu=1$ is filled with the rectangular-groove grating of height $h=50$ nm, period $d=a+b$ [a is the width of the filled stripes, and b is the spacing between the stripes], mark-to-space ratio $t=a/b=1$, and the stripes are filled with Ag, characterized by the 3D plasma frequency $\omega_p=5.69\times10^{15}$ s^{-1} and the phenomenological relaxation time $\tau=1.3165\times10^{-14}$ s. For the GaAs-$Ga_{1-x}Al_xAs$ SHS we use a homogeneous background dielectric constant to neglect image effects as done above in the calculation of the dispersion relations. Thus, layer $\nu=2$ is taken (only from the optical point of view) as a 10 nm thick GaAs layer (instead of $Ga_{1-x}Al_xAs$), characterized by the same background dielectric constant as that of layers $\nu=3$ and $\nu=4$: $\varepsilon_{s2}=\varepsilon_{s3}=\varepsilon_{s4}\equiv\varepsilon_s=12.87$. Layer $\nu=3$ contains the QW with the optically anisotropic (uniaxial) Q2DEG, characterized by a local diagonal dielectric tensor (for details, see Refs. 7 and 8) with plasma frequency $\omega_0=[n_{2DEG}e^2/(m_e\varepsilon_0\varepsilon_{s3}a_{2DEG})]^{1/2}$, where $a_{2DEG}=(8/5)[\hbar/(m_e\Omega_{10})]^2(\kappa_0+\kappa_1)\kappa_3^2\equiv d_3$ is the effective thickness of the Q2DEG, phenomenological longitudinal and transverse relaxation times $\tau_\parallel=\tau_\perp=1\times10^{-11}$ s, and oscillator strength $f_{10}=[\hbar/(m_e\Omega_{10})][8(\kappa_0\kappa_2)^3\kappa_3^2/(\kappa_0+\kappa_1)^6]$; region $\nu=4$ is the semi-infinite GaAs substrate, characterized by $\varepsilon_{s4}=\varepsilon_s$.

The quantity, usually extracted from FIR transmission experiments is the relative change in transmission of p-polarized light, $-\Delta T/T=1-T(n_{2DEG})/T(0)$, on which we focus the following discussion. The numerical results for the relative transmission coefficient are plotted in Fig. 4 for $\Theta_0=0°$ and different periods d of the grating. It is important to note that for the plotted frequency range and grating periods $d<26$ μm only the zeroth-order diffracted wave ($n=0$) is a propagating wave in the GaAs substrate, but for larger periods additionally the first-order diffracted waves ($n=\pm1$) become propagating waves. For $d=27.318$ μm the onset for the propagation of the first-order diffracted waves in the GaAs substrate takes place at $\omega=1.922\times10^{13}$ s^{-1} and results in the so-called Rayleigh anomaly[29] (for details, see Refs. 17 and 18), appearing as the tip in the relative transmission spectrum (see Fig. 4). Analyzing the spectra of Fig. 4 in detail, it becomes obvious that the maxima appearing for $d=20.940$ μm, $d=22.440$ μm, $d=24.166$ μm, and $d=26.100$ μm correspond to the lower intersubband plasmon-polariton branch ω_{pp}^{10-} at $q_\parallel=3.0\times10^3$ cm^{-1}, $q_\parallel=2.8\times10^3$ cm^{-1}, $q_\parallel=2.6\times10^3$ cm^{-1}, and $q_\parallel=2.4\times10^3$ cm^{-1}, respectively [see Fig. 2, where the symbols (●) represent these peak positions]. It is seen that the coupling efficiency of the incident FIR light with the mode ω_{pp}^{10-} increases with increasing d up to $d=26.100$ μm, where the largest magnitude of the maximum in $-\Delta T/T$ results. Increasing the period d, the line shape of the maximum becomes more and more asymmetric and, finally, transforms into a minimum. For $d=27.318$ μm a possible weak maximum cannot be distin-

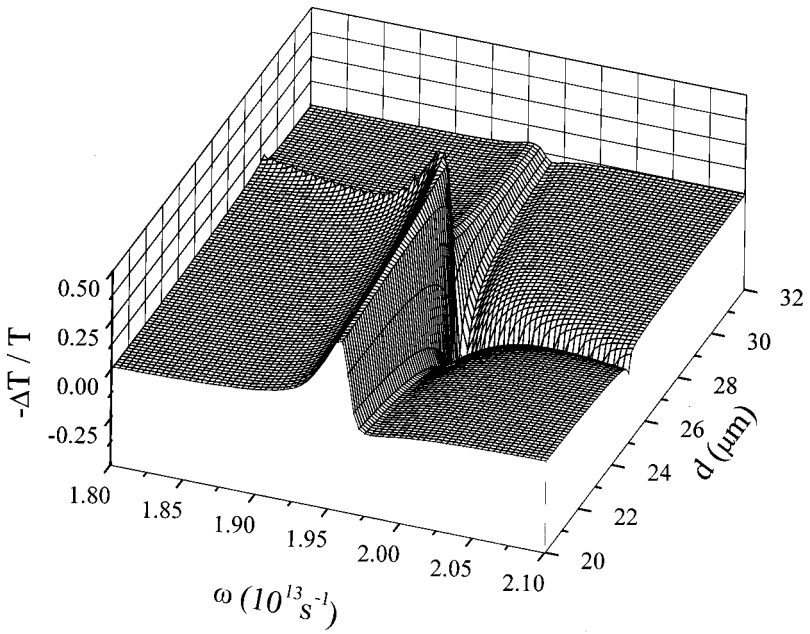

FIG. 6. 3D plot of the relative transmission coefficient $-\Delta T/T$ as a function of the frequency ω and the period d of the grating in the frequency range of the (1-0) intersubband plasmon polariton modes close to the onset of the Rayleigh anomaly for $\Theta_0=0°$. The calculation is performed for the multilayer system under consideration.

guished from the tip in the $-\Delta T/T$ spectrum representing the Rayleigh anomaly and the position of the minimum corresponds to the upper intersubband plasmon-polariton branch ω_{pp}^{10+} at $q_\parallel=2.3\times10^3$ cm^{-1}. Because ω_{pp}^{10+} is a radiative virtual mode, the energy radiation in the substrate causes $T(n_{2\mathrm{DEG}})>T(0)$. The transmission spectrum $T(n_{2\mathrm{DEG}})$ shows a maximum at the position of ω_{pp}^{10+} and this is the reason why we interpret the appearing minimum in $-\Delta T/T$ above the onset of the Rayleigh anomaly as caused by the excitation of the radiative virtual mode. In the cases of $d=28.560$ μm and $d=31.416$ μm only the minimum is observable in the spectra, corresponding to the upper mode ω_{pp}^{10+} at $q_\parallel=2.2\times10^3$ cm^{-1} and $q_\parallel=2.0\times10^3$ cm^{-1}, respectively.

In a recent paper we investigated the transformation of the line shape of the intersubband plasma mode (resonance) in relative transmission from a maximum with a Lorentzian line shape over a strongly asymmetric one to a minimum with increasing grating period.[17] In this paper we concluded that this deformation is caused by the Rayleigh anomaly (for the situation considered in the present paper), i.e., due to the onset of the propagation of the first-order diffracted waves in the substrate. Now, we are able to give a more precise explanation of this behavior: as long as the only propagating wave in the substrate is the zeroth-order wave, the relative transmission spectrum shows a maximum, responsible for the normal (1-0) intersubband plasmon mode ω_{pp}^{10-}, but after the onset of the Rayleigh anomaly, which itselfs appears only as a tip in the spectrum, the maximum disappears and a minimum, responsible for the radiative virtual (1-0) intersubband resonance ω_{pp}^{10+}, appears.

In Fig. 5 we show the relative transmission spectra for $d=27.318$ μm and different ray angles Θ_0. Because for $\Theta_0\neq0°$ the first-order diffracted waves $n=\pm1$ have different wave vectors, also two onsets for the Rayleigh anomaly occur at

$$\omega_R^{(n)}=\frac{2\pi c}{\sqrt{\varepsilon_s}d}\,\frac{|n|}{1\mp(\sin\Theta_0/\sqrt{\varepsilon_s})}$$

(see, e.g., the two tips at $\omega=1.906\times10^{13}$ s^{-1} and $\omega=1.938\times10^{13}$ s^{-1} in the spectrum for $\Theta_0=1.749°$), where the upper sign is valid for $n>0$ and the lower for $n<0$. Analyzing the spectra of Fig. 5, we can interpret the maximum for $\Theta_0=1.749°$ with the excitation of ω_{pp}^{10-} and the minimum with ω_{pp}^{10+}, both at $q_\parallel=2.32\times10^3$ cm^{-1} [the symbols (■) in Fig. 2 represent these peak positions]. Further, in the case of $\Theta_0=4.377°$ the same is true for $q_\parallel=2.35\times10^3$ cm^{-1} (◆) and also in the case of $\Theta_0=4.816°$ for $q_\parallel=2.355\times10^3$ cm^{-1} (not to distinguish in Fig. 2). For larger ray angles, however, the positions of the maxima and minima in the relative transmission spectra do not correspond to the dispersion relations of the modes. The reason for this result could be the very strong radiative damping of the upper mode ω_{pp}^{10+}. However, this rapid increase of the radiative damping above $q_\parallel=2.35\times10^3$ cm^{-1} (see Fig. 3) is not equivalently manifested in the relative transmission spectra.

To give a deeper inside in the effects appearing in the relative transmission spectrum in the frequency range of the $(1-0)$ intersubband plasmon mode close to the onset of the Rayleigh anomaly we show in Fig. 6 a 3D plot of $-\Delta T/T$ versus frequency ω and grating period d for the ray angle $\Theta_0=0°$ of the incident p-polarized light. The Rayleigh anomaly corresponds for frequencies below the (1-0) intersubband plasmon-polariton to the sharp maximum (corresponding to the tips in Fig. 4), which converts to the sharp minimum (i.e., the dips) for frequencies above $\omega_{pp}^{10\pm}$. Thus the Rayleigh anomaly which exactly corresponds to the light line in the GaAs substrate, $\omega=cq_\parallel/\sqrt{\varepsilon_s}$, extends from left to right on the $-\Delta T/T$ surface. Further, the lower mode ω_{pp}^{10-} corresponds to the maximum in $-\Delta T/T$ for grating periods below the onset of the Rayleigh anomaly and ω_{pp}^{10+} to the minimum above the onset of the Rayleigh anomaly. Thus the $-\Delta T/T$ surface plotted over ω and d gives a direct and impressive picture of the $\omega-q_\parallel$ plane, i.e., of Fig. 2.

In Fig. 7 we show a 3D plot of the relative transmission versus frequency ω and tilt angle Θ_0 for a fixed grating period $d=27.318$ μm. Here, the deep minimum correspond

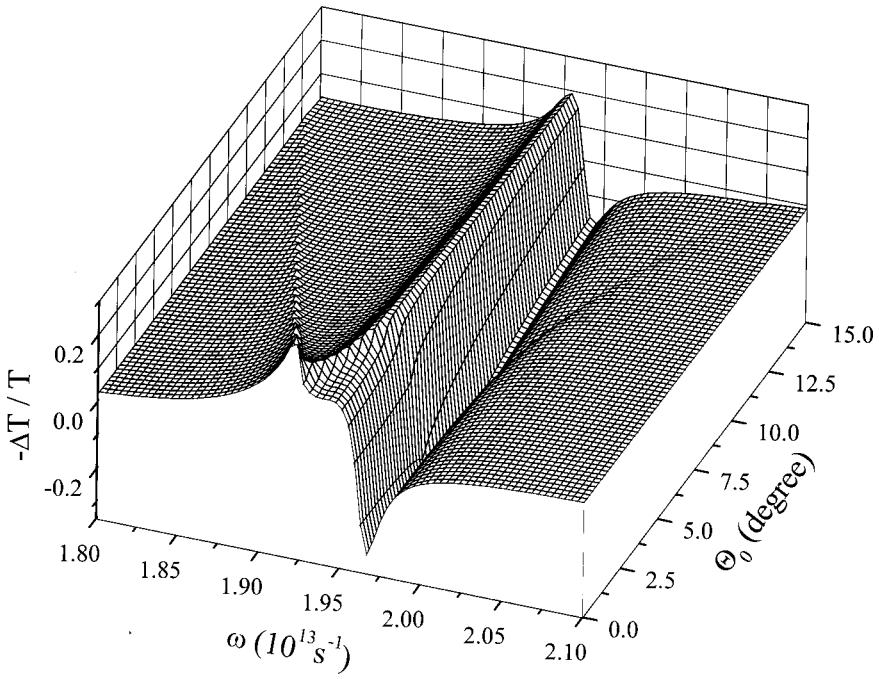

FIG. 7. 3D plot of the relative transmission coefficient $-\Delta T/T$ as a function of the frequency ω and the tilt angle Θ_0 in the frequency range of the (1-0) intersubband plasmon polariton modes close to the onset of the Rayleigh anomaly for $d=27.318$ μm. The calculation is performed for the multilayer system under consideration.

to the excitation of ω_{pp}^{10+} and the tips and dips appearing to the left and right of this minimum, respectively, correspond to the onsets of the Rayleigh anomaly due to the additional propagation of the first-order scattered waves $n=-1$ and $n=+1$
in the GaAs substrate. The tips appearing at smaller frequencies with increasing tilt angle correspond to the wave with $n=-1$ and the dips appearing at higher frequencies with increasing tilt angle correspond to the wave with $n=+1$.

Summarizing, we have shown that the intrasubband plasmon polariton is always a normal mode, whereas the intersubband plasmon polariton appears in two branches. The lower-frequency branch is a normal mode, but the higher-frequency branch is a radiative virtual mode. These modes appear in FIR transmission spectra: the normal modes correspond to maxima and the virtual mode corresponds to a minimum in the relative transmission. Because the radiative virtual intersubband resonance is only accessible in grating-coupler-assisted FIR transmission spectroscopy after the onset of the Rayleigh anomaly, the line-shape deformation of the intersubband resonance is caused by the excitation of this mode. Thus, we have shown that with the help of a grating, which produces the first-order light cone $\omega=(c/\sqrt{\varepsilon_s})\,|q_{\|}+(2\pi/d)|$ centered near the position of the retardation-induced resonance splitting of the modes, it should be possible to observe experimentally the influence of the retardation on the intersubband plasmon. For the chosen parameters minigaps due to Bragg scattering are not observed in the spectra.

[1] F. Stern, Phys. Rev. Lett. **18**, 546 (1967).
[2] A. V. Chaplik, Zh. Eksp. Teor. Fiz. **62**, 746 (1972) [Sov. Phys. JETP **35**, 395 (1972)].
[3] D. Dahl and L. J. Sham, Phys. Rev. B **16**, 651 (1977).
[4] L. Wendler and R. Pechstedt, Phys. Rev. B **35**, 5887 (1987).
[5] L. Wendler and R. Pechstedt, Phys. Status Solidi B **141**, 129 (1987).
[6] L. Wendler, R. Haupt, and V. G. Grigoryan, Physica B **167**, 91 (1990); **167**, 101 (1990); **167**, 113 (1990).
[7] L. Wendler and E. Kändler, Phys. Status Solidi B **177**, 9 (1993).
[8] L. Wendler and T. Kraft, Phys. Rev. B **54**, 11 436 (1996).
[9] S. J. Allen, Jr., D. C. Tsui, and R. A. Logan, Phys. Rev. Lett. **38**, 980 (1977).
[10] T. N. Theis, J. P. Kotthaus, and P. J. Stiles, Solid State Commun. **24**, 273 (1977).
[11] D. C. Tsui, E. Gornik, and R. A. Logan, Solid State Commun. **35**, 875 (1980).
[12] D. Heitmann, J. P. Kotthaus, and E. G. Mohr, Solid State Commun. **44**, 715 (1982).
[13] D. Olego, A. Pinczuk, A. Gossard, and W. Wiegmann, Phys. Rev. B **25**, 7867 (1982).
[14] E. Batke, D. Heitmann, and C. W. Tu, Phys. Rev. B **34**, 6951 (1986).
[15] K. D. Maranowski, A. C. Gossard, K. Unterrainer, and E. Gornik, Appl. Phys. Lett. **69**, 3522 (1996).
[16] T. N. Theis, J. P. Kotthaus, and P. J. Stiles, Solid State Commun. **26**, 603 (1978).
[17] L. Wendler, T. Kraft, M. Hartung, A. Berger, A. Wixforth, M. Sundaram, J. H. English, and A. C. Gossard, Phys. Rev. B **55**, 2303 (1997).
[18] L. Wendler and T. Kraft, Physica B **271** (1999).
[19] L. Wendler and R. Haupt, Phys. Status Solidi B **143**, 131 (1987).
[20] R. A. Ferrell, Phys. Rev. **111**, 1214 (1958).
[21] K. L. Kliewer and R. Fuchs, Phys. Rev. **150**, 573 (1966).

[22] K. L. Kliewer and R. Fuchs, Adv. Chem. Phys. **27**, 355 (1974).
[23] E. N. Economou and K. L. Ngai, Adv. Chem. Phys. **29**, 265 (1974).
[24] H. Raether, in *Physics of Thin Films*, edited by G. Hass, M. H. Francombe, and R. W. Hoffmann (Academic Press, New York, 1977), Vol. 9, p. 145.
[25] L. Wendler and R. Haupt, J. Phys. C **19**, 1871 (1986).
[26] A. A. Maradudin, in *Surface Polaritons*, edited by V. M. Agranovich and D. L. Mills (North-Holland, Amsterdam, 1982), p. 405.
[27] S. C. Kitson, W. L. Barnes, and J. R. Sambles, Phys. Rev. Lett. **77**, 2670 (1996).
[28] U. Mackens, D. Heitmann, L. Prager, J. P. Kotthaus, and W. Beinvogl, Phys. Rev. Lett. **53**, 1485 (1984).
[29] It should be noted that in general there are two types of grating (or Wood's) anomalies: (i) the Rayleigh wavelength-type and (ii) the resonance-type anomaly, which is connected with the excitation of a leaky surface wave propagating along the metallic grating. As shown in detail in Ref. 18 for the here discussed situation, the appearing tips and dips are caused by both types of Wood's anomalies. This is true because in the far-infrared frequency range, both types of Wood's anomalies occur at the same frequency and thus, cannot be distinguished. Because the onset of the Rayleigh wavelength-type anomaly is exactly determined by the onset (or disappearance) of a particular diffracted order of the propagating beam (in the substrate for transmission), in the present paper we call the appearing anomalies Rayleigh anomaly.